J. Fluid Mech. (2004), *vol.* 504, *pp.* 353–363. © 2004 Cambridge University Press
DOI: 10.1017/S002211200400789X Printed in the United Kingdom

An experimental study on stationary history effects in high-frequency Stokes flows

By C. F. M. COIMBRA[1], D. L'ESPERANCE[2], R. A. LAMBERT[3], J. D. TROLINGER[2] AND R. H. RANGEL[3]

[1]Department of Mechanical Engineering, University of Hawaii–Manoa, Honolulu, HI 96822, USA

[2]MetroLaser Incorporated, 2572 White Road, Irvine, CA 92614, USA

[3]Department of Mechanical and Aerospace Engineering, University of California, Irvine, CA 92826, USA

(Received 1 July 2003 and in revised form 23 December 2003)

We report results of a series of detailed experiments designed to unveil the dynamics of a particle of radius a moving in high-frequency, low-Reynolds-number oscillatory flow. The fundamental parameters in the problem are the Strouhal (Sl) and the particle Reynolds numbers (Re_p), as well as the fluid-to-particle density ratio α. The experiments were designed to cover a range of $SlRe_p$ from 0.015 to 5 while keeping $Re_p < 0.5$ and $Sl > 1$. The primary objective of the experiments is to investigate stationary history effects associated with the Basset drag, which are maximized when the viscous time scale a^2/ν is of the same order of the flow time scale $9/\Omega$, where 9 is a geometrical factor for the sphere, ν is the kinematic viscosity and Ω is the angular frequency of the background flow. The theoretically determined behaviour of stationary history effects is confirmed unequivocally by the experiments, which also validate the fractional derivative behaviour (of order 1/2) of the history drag for the range of parameters under study.

1. Introduction

The motion of particles in oscillatory flows is a physical phenomenon of importance to both industrial and natural processes. The mechanics of small particles in viscous flows is also the basis of much of the modern experimental work in fluid mechanics due to the widespread use of particle image velocimetry (PIV). From an experimental point of view, harmonic Stokes flows are ideal for studying history effects on particle dynamics because the sinusoidal forcing of the background flow continuously energizes the unsteady viscous layer surrounding the particle, thus generating a stationary history effect that can be measured continuously in time, as opposed to sudden accelerations or settling phenomena where the relative acceleration asymptotes to zero for long times (Hjelmfelt & Mockros 1966; Morrison & Stewart 1976; Chao 1968; Hinze 1975; Coimbra & Rangel 2001).

In order to model the physics of small particle motion in microgravity, Coimbra & Rangel (1998) produced the analytical solution to Tchen's equation of motion (Tchen 1947) for a particle that is allowed to move freely due to the action of a general time-dependent background flow, including initial transient effects. In a later publication on harmonic Stokes flow, Coimbra & Rangel (2001) focused on the role of the Basset history term and its relation to the other forces that depend on the relative velocity between the particle and the background flow (virtual mass and Stokes drag). The Basset history drag originates from a combination of the local acceleration and the viscous terms, and is shown to be maximum when the

https://doi.org/10.1017/S002211200400789X Published online by Cambridge University Press

dimensionless frequency $S = a^2\Omega/9\nu = SlRe_p \approx 1$, where a is the particle radius, ν the kinetic viscosity of the background flow and Ω its angular frequency. Coimbra & Rangel (2001) performed a scaling analysis to show that when $SlRe_p$ is much larger than unity, inviscid virtual mass effects dominate. The virtual mass force is associated with the local acceleration and pressure balance. When the virtual mass force dominates, the motion of the particle is virtually independent of the viscosity of the fluid. On the other hand, if $SlRe_p$ is much smaller than unity, the dominant force for a freely moving particle is the quasi-steady Stokes drag, a force that depends linearly on the viscosity of the fluid. The Strouhal and Reynolds numbers in our problem are defined as $Sl = a\Omega/9W_o$ and $Re_p = aW_o/\nu$, where the characteristic relative velocity W_o is taken as the product of the characteristic fluid velocity $\Omega\,\Delta x_f$ by the relative displacement ratio amplitude $1-\eta$, and η is the dimensionless particle-to-fluid displacement amplitude ratio $\Delta x_p/\Delta x_f$ so that $W_o = \Delta x_f \Omega\,(1-\eta)$.

Coimbra & Rangel (2001) and Coimbra & Kobayashi (2002) present a detailed discussion on the origin and contribution of each term to the viscous motion of a small particle, including a more detailed literature review of the problem. The primary objective of the present work is to obtain experimental verification of the predicted stationary history effects in high-frequency harmonic Stokes flows. Such experimental data providing insight into the behaviour of the history drag in high-frequency Stokes flow are not available in the literature, despite of a wealth of publications available on low-frequency high-Re_p flows. The present work also adds to prior studies in that the solitary particle is free to move with the oscillating background flow for very well-defined ranges of the relevant parameters Re_p and Sl.

2. Background

Tchen (1947) derived a Lagrangian equation of motion for a spherical particle freely moving in a uniform time-dependent background flow as a culmination of previous work attributed to Boussinesq (1885), Basset (1888) and Oseen (1927). Tchen's equation of motion can be written in terms of fractional operators (see Coimbra & Kobayashi 2002 for details):

$$\mathscr{D}(\boldsymbol{w}) + 3\hbar^{1/2}\,\mathscr{D}^{1/2}(\boldsymbol{w}) + \boldsymbol{w} = (\alpha - 1)\,\mathscr{D}(\boldsymbol{u}), \tag{2.1}$$

where $\boldsymbol{w} = \boldsymbol{v} - \boldsymbol{u}$ is the dimensionless relative velocity, α is the fluid-to-particle density ratio ρ_f/ρ_p and $\hbar \equiv \alpha/(2+\alpha)$. For a freely moving particle, velocities are made dimensionless by the relative characteristic velocity W_o. Time is made dimensionless by defining a particle characteristic time τ_p given by $a^2/9\nu\hbar$, so that a suitable dimensionless angular frequency $\omega = \Omega\tau_p$ can be used. The second (fractional) term on the left-hand side of (2.1) is the dimensionless Basset history term multiplied by a virtual mass coefficient. The differential operators in (2.1) are defined in a generic way (Coimbra & Kobayashi 2002) thus yielding physical insight into the response of the particle to a stationary flow forcing (Coimbra & Rangel 2001). We define the background flow velocity $\boldsymbol{u}$ as $\boldsymbol{A}e^{i\omega t}$, and the particle response $\boldsymbol{v}$ as $\boldsymbol{B}e^{i\omega t}$. With the identity $\mathscr{D}^{1/2}e^{i\omega t} = \sqrt{\omega}e^{i\omega t + \pi/4}$, a frequency analysis yields

$$\eta(S,\alpha) = \frac{|\boldsymbol{B}|}{|\boldsymbol{A}|} = \frac{\Delta x_p}{\Delta x_f} = \left|1 + \frac{(\alpha-1)(1-\hbar)iS}{iS + \hbar + 3\hbar\sqrt{S}e^{i\pi/4}}\right| = |\eta^*(S,\alpha)|, \tag{2.2}$$

where the term multiplying $e^{i\pi/4}$ in the denominator is directly associated with the history drag. The amplitude ratio η is used in this work to validate the theoretical predictions by comparing the measured values of η with (2.2) including or neglecting

https://doi.org/10.1017/S0022112004007899X Published online by Cambridge University Press

the last (history) term in the denominator. Note that due to details of the experimental setup described below, the comparison is made between the experimentally determined values of amplitude displacement and the real part of $\eta^*(S, \alpha)$.

Particle motion in oscillating flows has generated a significant amount of research activity. In sinusoidal background flow, it has been shown that the free particle motion in the stationary regime is represented by a sinusoidal wave as assumed above (Chao 1968; Hinze 1975; Martin, Padmanabhan & Ponce-Campos 1976; Coimbra & Rangel 2001). The harmonic motion of a sphere in a quiescent fluid has also been investigated (Stokes 1850; Landau & Lifshitz 1959; Odar & Hamilton 1964) and since the motion of the sphere in this case is prescribed, these studies represent a starting point for studies of suspended particles that are free to move in oscillatory flow. The most cited experiment on the dynamics of particles in oscillatory flow is the one by Odar & Hamilton (1964). However, the analysis of the experimental results conducted by Odar & Hamilton incurs conceptual errors due to limited theoretical insight available at the time. During a subsequent and more careful analysis of the same experiments and other theoretical results, Mei & Adrian (1992) showed that the empirical expressions for the history and virtual mass coefficients originally proposed by Odar & Hamilton failed to correctly account for nonlinearities of the flow at finite Re_p.

The connection between maximum history drag effects and the dimensionless local acceleration $S = SlRe_p$ is significant because it is common practice to neglect the effects of the unsteady drag in experiments of time-dependent flow and isotropic turbulence (Houghton 1963; Mei, Adrian & Hanratty 1991*a*; Mei, Lawrence & Adrian 1991*b*). In unsteady Stokes flow, a condition for neglecting convective terms is that $SlRe_p$ be larger than unity so that $SlRe_p > Re_p$ (Mei & Adrian 1992; Lovalenti & Brady 1993; Coimbra & Kobayashi 2002). Coimbra & Rangel (2001) also showed that for a particle to remain in the Stokes regime ($Re_p < 1$) with $Sl > 1$, the background fluid displacement must be much smaller than the radius of the particle. Numerical simulations of oscillatory flow past a fixed sphere, a problem related to the one investigated here, also provide insight into the role of the history term at finite Re_p (Mei & Adrian 1992; Chang & Maxey 1994). Kim, Elghobashi & Sirignano (1998) studied numerically the case of a heavy ($\alpha < 0.2$) free particle in the range of $Re_p > 1$.

3. Experiments

In the experiments, we examine the motion of spherical particles tethered to a fluid cell that is oscillating sinusoidally. Since the movement of a spherical particle in response to the surrounding fluid is predicted by the stationary solution of the particle equation of motion, we test the theory by measuring the response of the particle to the fluid motion. Specifically, we measure the ratio of the particle-to-fluid displacement η at different forcing frequencies.

3.1. *Experimental apparatus*

An electromagnetic shaker, as sketched in figure 1, drives the liquid-filled cell at frequencies ranging from 10 to 80 Hz. The cubic cell is a 4 cm cube inside, with two windows on opposing faces for optical access. The cell is large enough to prevent interactions between a 2 mm radius particle placed in the centre of the cell and the cell walls at the given frequencies. In several experiments, an additional wall was placed in the centre of the cell near the particle to examine the effects of particle and wall interactions. The cell is sealed to ensure solid body motion of the fluid in the far field and to eliminate air bubbles, since movement of gas–liquid surfaces generates currents

https://doi.org/10.1017/S002211200400789X Published online by Cambridge University Press

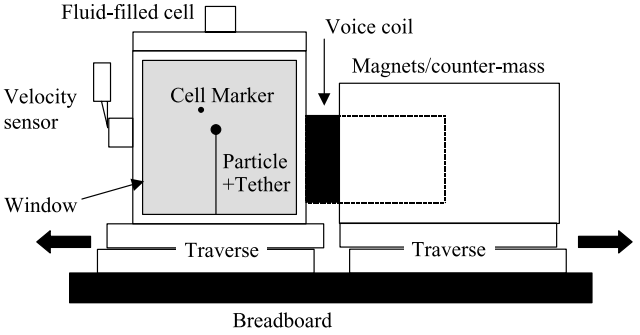


FIGURE 1. Diagram of the electromagnetic shaker.

within the liquid. Several preliminary tests of the apparatus show that oscillations of the cell do not produce currents, thus ensuring that motion of the fluid is equivalent to that of the cell.

The cell is mounted on a single-axis traverse to constrain the vibration along a single direction. Two counteracting springs are used to centre the transverse. An electromagnetic voice coil actuator oscillates the cell in a sinusoidal motion with single mode frequencies from 10 to 80 Hz at amplitudes ranging between 75 and 200 μm. The recoil from the motion of the test cell is significant and was found to cause severe vibration of the experimental platform and optics when the voice coil magnets were mounted directly to the experimental platform. To absorb the recoil, the magnets are held within a brass counter-mass block which is mounted on a second traverse; the total mass of the counter-mass plus magnets is approximately 13 times that of the test cell plus voice coil. A phonograph needle in contact with the cell registers the cell velocity. Motion of the needle flexes a piezoelectric crystal, producing a voltage that is proportional to velocity. A spectrum analysis of the velocity signals at the frequencies used in the experiment showed that almost all of the cell oscillation is at the fundamental frequency with very little distortion. Distortion comprises mainly second and third harmonics of the fundamental mode, which are at least three hundred times less intense than the fundamental mode in our experiments.

3.2. *Measurement techniques*

In order to calculate the particle-to-fluid displacement amplitude ratio η, two quantities were measured in each experimental trial: the amplitude of the cell displacement (AT), and the amplitude of the particle displacement (AP) during a single oscillation of the cell. The displacements are measured using digital images of the particle and a cell reference marker that are recorded at the two extremes of the cell oscillation. The stationary solution of the particle equation of motion predicts a small phase delay or advance between the cell motion and the particle motion, thus the particle does not reach the limit of displacement at the same time that the cell does. The predicted phase difference is smaller than the shutter opening time and it is therefore impractical to use the present experimental setup to measure the particle and cell positions when the cell velocity is high. When the particle reaches the maximum displacement, the velocity approaches zero and the change in distance resulting from the phase lag is less than 2 μm. In order to properly account for the small phase difference between the fluid cell and the particle we compare the experimental results with the real part of $\eta^*(S, \alpha)$ since the measurements record only the amplitude ratio at the maximum of the fluid oscillation (see (2.2)). The difference

https://doi.org/10.1017/S002211200400789X Published online by Cambridge University Press

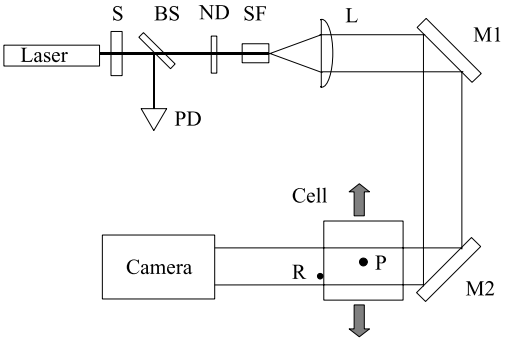


FIGURE 2. Optical layout of the experiment.

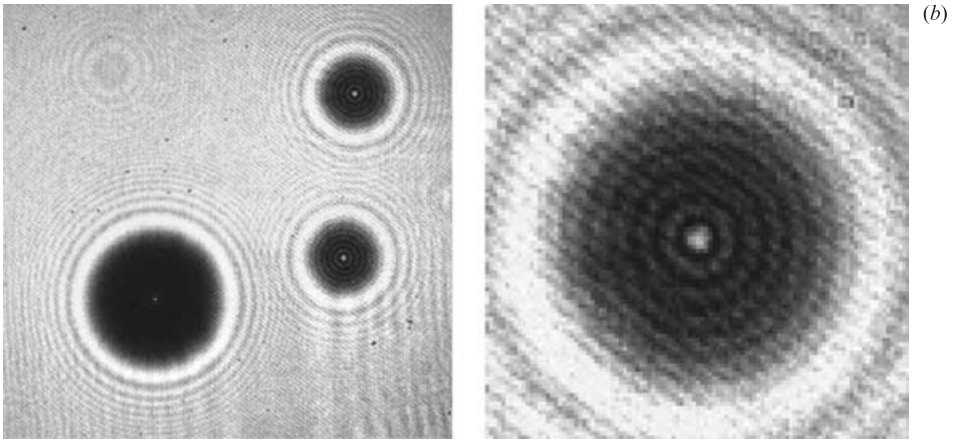


FIGURE 3. A digital image of the diffraction patterns within the cell. The large circular object in (*a*) is the shadow of a 1 mm radius spherical particle floating within the fluid with two smaller circular objects that are the reference markers with a radius of 0.5 mm. A magnified view of one of the shadows in (*b*) shows several rings surrounding the Poisson spot. The diagonal stripe pattern is the interference from the cell windows.

between the absolute value of $\eta^*(S, \alpha)$ and its real component is negligible ($< 1\%$) for the lighter set of particles used in the experiments ($\alpha \approx 2$) and small (2–8%) for the heavier particles ($\alpha \approx 0.1$) over the range of frequencies under study.

A schematic diagram of the optical system is provided in figure 2. The illumination source is a 10 mW HeNe laser modulated by a shutter (S). A beam-splitter (BS) diverts a small amount of the light into a photodiode (PD) to monitor the opening of the shutter. The illumination intensity is adjusted by a neutral density filter (ND), then spatially filtered (SF) and collimated by a lens (L). Two mirrors (M1 and M2) aim the de-focused beam at normal incidence through the cell, which oscillates horizontally. A 0.5 mm radius sphere (R) is glued to the back window of the cell to serve as a cell reference marker. The particle (P) is enclosed within the fluid-filled cell. The shutter opens for 0.8 ms at each of the two extremes of cell motion, when the cell velocity is zero, and two digital images of the cell are recorded by an 8-bit, 1024 by 1024 pixel CCD camera (Kodak MegaPlus ES 1.0). Each pixel has an edge length of 9 μm. No lens is used on the camera; the field of view is limited to the central 1 cm^2 of the cell. The camera is located between 15 and 18 cm behind the second cell window so that the particle shadow creates a distinct Fresnel diffraction pattern, as shown in figure 3.

https://doi.org/10.1017/S002211200400789X Published online by Cambridge University Press

Quantity	$\alpha \sim 2$	$\alpha \sim 1$	$\alpha \sim 0.1$
Fluid	Krytox	Krytox + $C_5H_2F_{10}$	mineral oil
Fluid density	1.89 g cm^{-3}	1.85–1.86 g cm^{-3}	0.86 g cm^{-3}
Viscosity	40 cS	27 cS	185 cS
Particle material	polypropylene	magnesium alloy	brass
Particle radius	0.5, 1.0, 2.0 mm	1.0 mm	1, 1.6, 2 mm
Particle density	0.90–1.03 g cm^{-3}	1.86 g cm^{-3}	8.6 g cm^{-3}
Tether material		copper wire	
Tether density		8.9 g cm^{-3}	
Tether diameter		19 μm	
Tether length		2.0 cm	
Cell amplitude		75–100 μm	
Frequency range		10–80 Hz	

TABLE 1. Experimental parameters.

We use the Fresnel diffraction pattern to locate the centre of the particle position to within a fraction of a pixel. The bright spot at the centre of the diffraction pattern (known as Poisson's spot) and the surrounding rings provide an excellent-noise free predictable light pattern that is used as a correlation template. For the region of the shadow within half a radius of the centre, the intensity I(x, y) of a pixel with coordinates (x, y) is described as (Trolinger *et al.* 2003):

$$I(x, y) = I_o J_o^2\left(\frac{\pi\sqrt{(x - x_o)^2 + (y - y_o)^2}}{\sigma}\right), \tag{3.1}$$

where I_o is a normalization constant, J_o is the zeroth-order Bessel function, σ is the ring spacing, and (x_o, y_o) are the coordinates of the pattern centre. The location of the pattern centre in a digital image is determined by first analysing the images to determine σ and I_o, then generating a template pattern similar to that in (3.1), cross-correlating the template with the image, and finally locating the maximum of the cross-correlation. The algorithm that locates the centre is briefly described in an earlier paper (Trolinger *et al.* 2003). We tested the algorithm by analysing composed digital images of ideal Fresnel diffraction patterns superimposed onto noisy backgrounds. The program can locate the centre of the particle or reference marker to within 0.1 pixel (1 μm). The combined uncertainty in the particle position due to the phase lag and uncertainty locating the center is 2.2 μm.

3.3. *Experimental parameters*

The magnitudes of the experimental parameters correspond to a low-Re_p flow regime where the effect of the history term peaks. The experimental parameters, such as the tether and particle dimensions, density ratio, and fluid viscosity, are given in table 1 for the various experiments. Krytox (perfluoroalkylether) and mineral oil are used as fluids in the experiment because they are optically transparent, have low flammability, low toxicity, and high viscosity. In order to test the influence of the particle-to-fluid density ratio on particle motion, three different cases are examined: polypropylene ($\alpha = 2.1$) or polystyrene ($\alpha = 1.8$) in Krytox, magnesium alloy in a mixture of Krytox and decafluoropentane ($\alpha = 1.0$), and brass in mineral oil ($\alpha = 0.1$). The experiments are conducted using particle radii ranging from 0.5 to 2.0 mm. Tethers with lengths of 2.0 cm are used to anchor these particles to either the bottom or top of the cell. We

https://doi.org/10.1017/S002211200400789X Published online by Cambridge University Press

tested several different tether materials including human hair, spider web filaments, and thin nylon thread before identifying 19 μm diameter copper wire as the best choice for a tether in our experiments.

4. Results and discussion

4.1. *Tether effects*

Due to the relatively small size of the experimental apparatus and the spheres used in the experiment, the influence of the tether drag on particle motion is of some concern. During the experiments, the oscillations of the sphere are small enough such that the angle swept by the tether is very small, thus allowing a simplified analysis. The drag on a thin tether is approximated using the equation for a cylinder of length L_c and diameter d in low-Reynolds-number flow under steady conditions. For flow normal to the axis, the steady drag is roughly $10Re_c^{-0.8}$, where $Re_c = W_c d/\nu$ (Clift, Grace & Weber 1978). For the sphere, the Stokes drag equation is used. The maximum (or characteristic) relative velocity of the sphere, $W_o = \Omega \Delta x(1-\eta)$ is calculated using experimental data on the relative displacement and the angular frequency Ω of the fluid oscillations. To account for one end of the tether being held fixed at the cell floor or ceiling, the relative velocity of the tether is assumed to be half of the relative velocity of the particle. Using these approximations, the drag ratio between the tether and the sphere is estimated to be

$$r_d = 0.13Re_c^{0.2}L_c/a, \tag{4.1}$$

which is strictly valid for $Re_c \ll 1$. Equation (4.1) shows that the drag ratio is directly proportional to the ratio of the tether length to the radius of the sphere, and weakly proportional to the tether diameter through the $Re_c^{0.2}$ dependence. The order of magnitude analysis for thin tethers that results in (4.1) indicate that tether effects in our experiments fall within the overall experimental uncertainty, and therefore play a negligible role in the measurements for the displacement amplitude. This assertion is corroborated by the agreement between theory and experiments for a wide range of frequencies and particle sizes when the thinnest tether was used.

We performed several control experiments to characterize the effects of tether thickness and length, concentrating mostly on the oscillation of (free and tethered) neutrally buoyant particles, and observed a significant effect when tethers were thick. Neutral buoyancy was achieved by suspending magnesium alloy particles (density $= 1.86\ \mathrm{g\ cm^{-3}}$) in a mixture of Krytox and decafluoropentane having a density equal to that of the particles. For the free particles, the particle response ratio was 1.000 ± 0.006 at all cell oscillation frequencies, as predicted by theory. In contrast, the particle response ratio was 0.96 ± 0.01 for particles tethered by a human hair having an approximate diameter of 100 μm. The results from the control experiments drove us to seek ever thinner and more flexible tethers. Tests with neutrally buoyant particles tethered by 50 μm diameter nylon tethers gave an average particle response ratio of 0.99 ± 0.02. Experiments with 1 mm radius polypropylene particles in Krytox ($\alpha = 2.1$) tethered by 2 cm long tethers also show evidence of tether effects, which tend to reduce the particle response ratio as the tether becomes thicker and the drag ratio increases. At 70 Hz, the measured particle response was 1.090 ± 0.011 for a particle tethered by 100 mm diameter hair, 1.156 ± 0.015 for a particle tethered by 50 μm diameter nylon thread, and 1.179 ± 0.021 for a particle tethered by 19 μm diameter copper wire. The η-value obtained with the copper wire tether is closest to the predicted value of $\eta = 1.18$ for a 1 mm radius $\alpha = 2.1$ particle.

https://doi.org/10.1017/S002211200400789X Published online by Cambridge University Press

We examined the effect of small changes in the tether length by measuring the displacement ratios obtained from 1 mm radius $\alpha = 2.1$ particles tethered by three different lengths of 50 μm diameter fibre: 1.5, 2.0, and 2.5 cm. No significant differences were observed. With the control experiments and the estimate of the drag ratio given by (4.1), we are confident that tether effects do not affect our conclusions.

4.2. *Particle–wall and particle–particle interactions*

To characterize the interactions between particles and walls, we examined the response of a 2 mm radius particle with $\alpha = 2.1$ at three different locations within the cell. In the first case, the particle was located near the centre of the cell. In the second case, the centre of the particle was located about 4 mm from a sidewall such that the cell motion was perpendicular to the wall. In the third case, the centre of the particle was located about 4 mm from a window, such that the cell motion was parallel to the window. The measured frequency dependence of η was approximately the same for all three cases, and is also approximately equal to the theoretically predicted curve for a lone particle in an infinite body of fluid. The results suggest that wall effects have little influence on high-frequency particle displacement unless the particle is less than 2 radii away from the wall.

To characterize interactions between particles, we measured the displacement ratio, at frequencies ranging from 10 to 80 Hz, of two tethered particles with radii of 1 mm and $\alpha = 2.1$ that were separated from each other by 4 mm (centre to centre) along the direction of motion. The measured response values for the two particles were equal to each other (within the experimental uncertainty) and to the theoretically predicted values for a single unperturbed particle with the same radius and relative density. This result shows that particles separated by more than 2 radii of distance have little influence on the overall motion of the adjacent particle for the range of $SlRe_p$ under study, particularly when $SlRe_p > 1$.

The weak influence of adjacent particles and walls for distances larger than 2 radii agrees well with the expectation for high-frequency motion characterized by $SlRe_p \approx 1$, since a dimensionless penetration depth δ can be estimated to be of order $(\nu/\Omega)^{1/2}$ (see e.g. Landau & Lifshitz 1959). A dimensionless penetration depth for our geometry is $\delta/a \approx (9\nu/\Omega a^2)^{1/2} \approx (SlRe_p)^{-1/2}$. Therefore, the expected range of influence δ is of the order of the particle radius for $SlRe_p \approx 1$. Note also that when $\alpha \to 1$, the characteristic relative velocity W_o asymptotes to zero, and the concept of a penetration depth based on the time scale is immaterial because $Sl \to \infty$, despite the fact that the product $SlRe_p$ remains finite.

4.3. *Amplitude response of the particles*

The response of polypropylene ($\alpha = 2.1$) particles in Krytox in shown on figure 4(*a*). Two different radii of polypropylene particles are used: 1.00 and 1.98 mm. In addition, we also examined the response of 0.5 mm radius polystyrene particles ($\alpha = 1.8$), since 0.5 mm radius polypropylene particles were not available. Figure 4(*a*) shows a plot of the displacement ratio η as a function of dimensionless frequency $S = SlRe_p$ for $1.835 < \alpha < 2.1$. The upper thin curves correspond to the solution without the history term for $\alpha = 2.1$ (the top curve) and for $\alpha = 1.835$ (the second curve from the top). The thick curves correspond to the full solution for the same limiting cases.

The response of brass particles in mineral oil ($\alpha = 0.1$) is studied as an example where the particles are denser than the fluid. A plot of the displacement ratio versus the normalized frequency is shown on figure 4(*b*). Three different particle radii are used in the experiment: 1.00, 1.59, and 1.98 mm. The lower thin curve corresponds to the

https://doi.org/10.1017/S002211200400789X Published online by Cambridge University Press

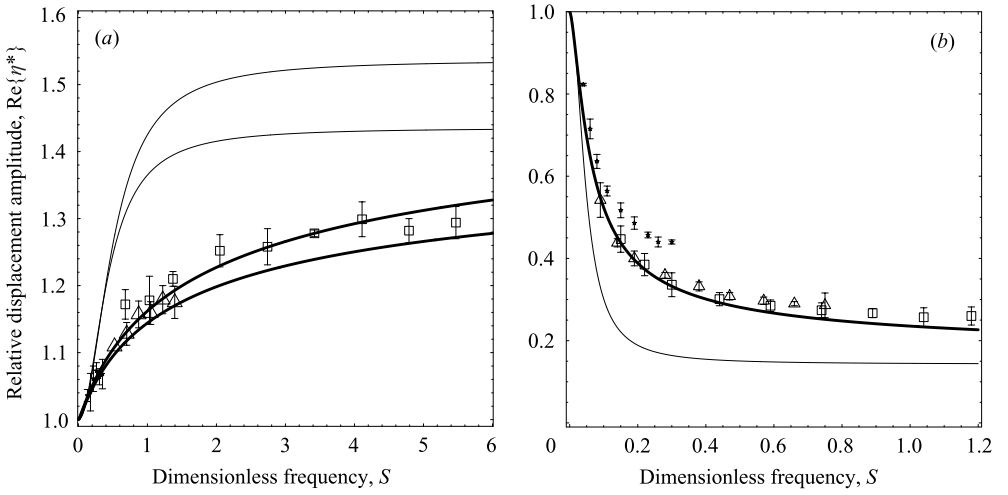


FIGURE 4. Comparison of experimental and theoretical results for the relative displacement amplitude $\mathrm{Re}\{\eta^*\}$ as a function of the dimensionless frequency S. (*a*) Results for $1.835 < \alpha < 2.100$. Symbols: ● (left bottom corner) are for (a, α) equal to (0.500 mm, 1.835); △ (1.00 mm, 2.077); □, (1.98 mm, 2.100). (*b*) As (*a*) but for $\alpha = 0.1 \pm 0.001$: ● (a, α) equal to (1.00 mm, 0.100); △ (1.59 mm, 0.099); □ (1.98 mm, 0.099). The solid lines indicate analytical solutions including history effects (thick) and excluding history effects (thin). The top curves of each type on (*a*) refer to $\alpha = 2.100$ and the lower curves of each type refer to $\alpha = 1.835$.

analytical solution without the history drag for $\alpha = 0.1$. The thick curve corresponds to the full solution – where the history force is included – for the same case. For $S > 0.1$, the difference between the two curves is pronounced due to the importance of the history force at dimensionless frequencies between 0.1 and 10 (Coimbra & Rangel 2001). The measured particle response closely matches the theoretical predictions for the full solution, and is clearly different from the solution where the history force is neglected.

The experiments show that the theory predicts the amplitude displacement of the light particles ($\alpha \approx 2$) within 2% of error (see figure 5*a*) when history effects are included. Without history effects the error is of the order of 20%. For the heavy particles, the experiments match the theory within 15–20% when history effects are included. Without history effects, the average error is 40–60% for values of $S > 0.2$. The larger error for $\alpha \approx 0.1$ is attributed to three factors. First, the displacement of heavy particles is smaller and thus the systematic errors in the experiment are more evident for such small displacements. We consider this factor the primary cause for error. Second, tether effects may be more pronounced when α deviates from unity because the tension in the tether is higher. However, our estimates show that this contribution is of secondary importance. Finally, and to a lesser degree, the Strouhal number Sl for the heavy particles is smaller, and thus the theory is expected to be less accurate in this case (figure 5*b*). Nonetheless, the experiments clearly show a very strong agreement with the theory when history drag effects are included, and a very poor agreement when history effects are removed. Also, the relative errors show no clear tendency to be smaller for small $SlRe_p$ when history contributions are considered, which indicates that the scattering of the data for heavy particles is mostly due to systematic experimental errors. The experiments strongly support the validity of Tchen's equation for $Re_p < 0.5$ and $Sl > 1$ for both heavy and light particles.

https://doi.org/10.1017/S002211200400789X Published online by Cambridge University Press

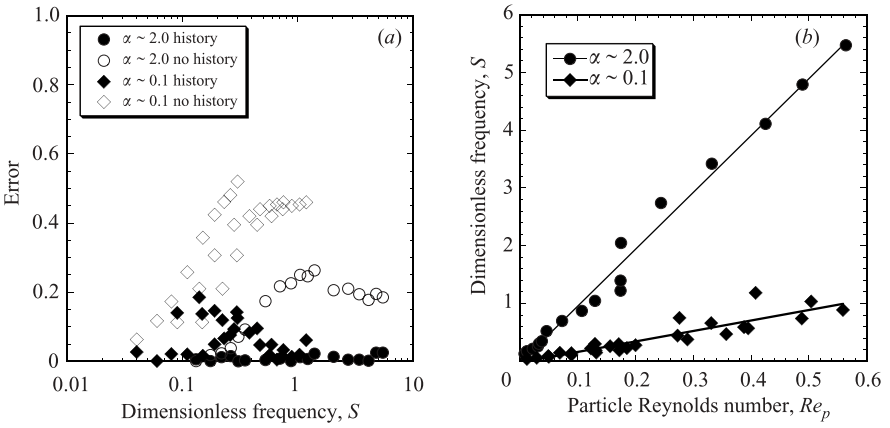


FIGURE 5. (*a*) Relative error between theory and experiments($|\eta_{theory} - \eta_{exp}|/\eta_{exp}$) as a function of the dimensionless frequency $S = Sl Re_p$. (*b*) Measured values of $Sl Re_p$ versus Re_p. The slope of the curve is Sl for the two different density ratios ($Sl(0.1) \approx 1.8$ and $Sl(2) \approx 9.8$).

5. Conclusions

A series of experiments on solitary particle motion in high-frequency oscillatory flow was conducted in order to evaluate stationary history effects. The experiments show unequivocal agreement with the theory (errors less than 2%) for light particles ($1.8 < \alpha < 2.1$) and moderately good agreement with the theory (errors typically less than 15%) for heavy particles ($\alpha = 0.1$) for the range of $Re_p < 0.5$ and $Sl > 1$. The larger errors in the case of heavy particles are attributed mainly to systematic measurement errors and not to failure of the theory or tethering effects. When history drag effects are ignored, the deviation between theory and experiments increases by one order of magnitude for light particles and by a factor of 3–5 for heavy particles, well beyond the experimental uncertainty associated with the experiments. For the range of parameters investigated in this work, particle–wall and particle–particle effects were found to be negligible for distances larger than 2 radii, a result that deviates substantially from the large region of influence associated with steady creeping flows. The smaller region of influence at high frequencies is expected due to the increased importance of near-field effects generated by the local acceleration term ($Sl Re_p$).

This is work is supported by NASA's flight definition project SHIVA (Spaceflight Holography Investigation in a Virtual Apparatus) under contract number NAS8-98091. The NASA management team includes M. Bodiford, Project Manager, Dr D. Smith, Project Scientist, W. Patterson, Systems Engineer, all from NASA's MSFC. The authors wish to acknowledge M. Dempsey of MetroLaser for conducting much of the experimental work.

REFERENCES

BASSET, A. B. 1888 On the motion of a sphere in a viscous liquid. *Phil. Trans. R. Soc. Lond.* A **179**, 43–63.

BOUSSINESQ, J. 1885 Sur la résistance qu'oppose un liquide indéfini en repos, sans pesanteur, au mouvement varié d'une sphère solide qu'il mouille sur toute sa surface, quand les vitesses restent bien continues et assez faibles pour que leurs carrés et produits soient négligeables. *C. R. Acad. Sci. Paris* **100**, 935–937.

https://doi.org/10.1017/S002211200400789X Published online by Cambridge University Press

Chang, E. J. & Maxey, M. R. 1994 Unsteady flow about a sphere at low to moderate Reynolds number. Part 1. Oscillatory motion. *J. Fluid Mech.* **277**, 347–379.

Chao, B. T. 1968 Turbulent transport behavior of small particles in dilute suspension. *Ósterreichisches Ing.-Archiv* **18**, 7–21.

Clift, R., Grace, J. R. & Weber, M. E. 1978 *Bubbles, Drops, and Particles*. Academic.

Coimbra, C. F. M. & Kobayashi, M. H. 2002 On the viscous motion of a small particle in a rotating cylinder. *J. Fluid Mech.* **469**, 257–286.

Coimbra, C. F. M. & Rangel, R. H. 1998 General solution of the particle momentum equation in unsteady Stokes flow. *J. Fluid Mech.* **370**, 53–72.

Coimbra, C. F. M. & Rangel, R. H. 2001 Spherical particle motion in harmonic Stokes flows. *AIAA J.* **39**, 1673–1682.

Hinze, J. O. 1975 *Turbulence*. McGraw-Hill.

Hjelmfelt, A. T. & Mockros, L. F. 1966 Motion of discrete particles in turbulent fluid. *Appl. Sci. Res.* **16**, 148–161.

Houghton, H. 1963 The behaviour of particles in a sinusoidal velocity field. *Proc. R. Soc. Lond.* A **272**, 33–43.

Kim, I., Elghobashi, S. E. & Sirignano, W. A. 1998 On the equation of motion for spherical-particle motion: effects of Reynolds and acceleration numbers. *J. Fluid Mech.* **367**, 221–253.

Landau, L. D. & Lifshitz, E. M. 1959 *Fluid Mechanics*. Pergamon.

Lovalenti, P. M. & Brady, J. F. 1993 The hydrodynamic force on a rigid particle undergoing arbitrary time-dependent motion at small Reynolds number. *J. Fluid Mech.* **256**, 561–605.

Martin, C. S., Padmanabhan, M. & Ponce-Campos, C. D. 1976 Rolling motion of a sphere on a plane boundary in oscillatory flow. *J. Fluid Mech.* **76**, 653–674.

Mei, R. W. & Adrian, R. J. 1992 Flow past a sphere with an oscillation in the free-stream velocity and unsteady drag at finite Reynolds number. *J. Fluid Mech.* **237**, 323–341.

Mei, R. W., Adrian, R. J. & Hanratty, T. J. 1991*a* Particle dispersion in isotropic turbulence under Stokes drag and Basset force with gravitational settling. *J. Fluid Mech.* **225**, 481–495.

Mei, R. W., Lawrence, C. J. & Adrian, R. J. 1991*b* Unsteady drag on a sphere at finite Reynolds number with small fluctuations in the free-stream velocity. *J. Fluid Mech.* **233**, 613–631.

Morrison, F. A. & Stewart, M. B. 1976 Small bubble motion in an accelerating fluid. *J. Appl. Mech.* **97**, 399–402.

Odar, F. & Hamilton, W. S. 1964 Forces on a sphere accelerating in a viscous fluid. *J. Fluid Mech.* **18**, 302–314.

Oseen, C. 1927 *Hydromechanik*. Leipzig: Akademische Verlag.

Stokes, G. G. 1850 On the effect of internal friction of fluids on the motion of pendulums. *Trans. Camb. Phil. Soc.* **9**, 8–106.

Tchen, C. M. 1947 Mean value and correlation problems connected with the motion of small particles suspended in a turbulent fluid. Doctoral dissertation, Delft University, The Hague.

Trolinger, J. D., L'Esperance, D., Rangel, R. H., Coimbra, C. F. M., Witherow, W., Bodiford, M. & Patterson, B. 2003 Ground-based and mockup experiments to support the ISS flight definition program SHIVA. *Proc. 2003 IEEE Aerospace Conf., 8–16 March 2003 – Big Sky, MT*.

https://doi.org/10.1017/S002211200400789X Published online by Cambridge University Press